International Journal of Fracture (2005) 131:189–209
DOI 10.1007/s10704-004-3948-6

Continuum shape sensitivity and reliability analyses of nonlinear cracked structures

SHARIF RAHMAN* and GUOFENG CHEN
Department of Mechanical Engineering, The University of Iowa, Iowa City, IA 52242, (Phone: (319) 335-5679; Fax: (319) 335-5669)
**Author for correspondence. (E-mail: rahman@engineering.uiowa.edu)*

Received 23 December 2002; accepted in revised form 28 August 2004

Abstract. A new method is proposed for shape sensitivity analysis of a crack in a homogeneous, isotropic, and nonlinearly elastic body subject to mode I loading conditions. The method involves the material derivative concept of continuum mechanics, domain integral representation of the *J*-integral, and direct differentiation. Unlike virtual crack extension techniques, no mesh perturbation is required in the proposed method. Since the governing variational equation is differentiated before the process of discretization, the resulting sensitivity equations are independent of any approximate numerical techniques. Based on the continuum sensitivities, the first-order reliability method was employed to perform probabilistic analysis. Numerical examples are presented to illustrate both the sensitivity and reliability analyses. The maximum difference between the sensitivity of stress-intensity factors calculated using the proposed method and the finite-difference method is less than four percent. Since all gradients are calculated analytically, the reliability analysis of cracks can be performed efficiently.

Key words: Crack, energy release rate, *J*-integral, nonlinear fracture mechanics, probabilistic fracture mechanics, and reliability, shape sensitivity analysis.

1. Introduction

In stochastic fracture mechanics, the derivatives of the *J*-integral or other fracture parameters are often required to predict the probability of fracture initiation and/or instability in cracked structures (Madsen et al., 1986; Provan, 1987; Besterfield et al., 1990; Grigoriu et al., 1990; Besterfield et al., 1991; Rahman, 1995; Rahman and Kim, 2000; Rahman, 2001). The calculation of these derivatives with respect to load or material parameters, which constitutes size-sensitivity analysis, is not unduly difficult. However, the evaluation of derivatives with respect to crack size is a challenging task, since it requires a shape sensitivity analysis. Using a brute-force type finite-difference method to calculate shape sensitivities of crack-driving forces is often computationally expensive, because numerous deterministic analyses by the finite element method (FEM) may be required for a complete reliability analysis.[1] Furthermore, if the finite-difference perturbations are too large relative to FEM meshes, the approximations

[1]Here the finite-difference method refers to the calculation of derivatives of a performance function, e.g., the *J*-integral, with respect to the crack size; the finite element method refers to the solution of the boundary-value problem for a given crack size.

can be inaccurate, whereas if the perturbations are too small, numerical truncation errors may become significant. Therefore, for any deterministic or probabilistic fracture analysis that significantly depends on shape sensitivities, it is important to evaluate the derivatives of fracture parameters accurately and efficiently. In this paper, the shape sensitivity analysis refers to the first-order derivative of a crack-driving force with respect to the crack size.

In the linear-elastic fracture mechanics, some methods have already appeared to predict the sensitivities of stress-intensity factors (SIFs) with respect to the crack size. These methods entail two fundamental approaches: (1) the virtual crack extension approach and (2) the continuum shape sensitivity approach. In the first approach, Lin and Abel (1988) introduced a variational formulation in conjunction with a virtual crack extension technique (delorenzi, 1982, 1985; Haber and Koh, 1985; Barbero and Reddy, 1990) (primarily used for calculating SIFs indirectly) to calculate the first-order derivative of SIF for a single crack. Later, Suo and Combescure (1992) developed a double virtual crack extension method to calculate the first-order sensitivity of the energy release rate (ERR) with respect to the crack size. This method cleverly avoids calculation of the second-order derivative of the stiffness matrix and is applicable under combined loading conditions. Subsequently, Hwang et al. (1998) generalized the virtual crack extension method to calculate both first- and second-order derivatives of SIFs for linear structures involving multiple cracks, crack-face pressure, and thermal loading. However, all of these methods in this approach require a mesh perturbation, a fundamental drawback of all virtual crack extension techniques. For higher-order derivatives, the number of elements affected by mesh perturbation surrounding the crack tip has a significant effect on the solution accuracy (Hwang et al., 1998).

Recently, alternative methods based on continuum shape sensitivity theory have emerged to obtain derivatives of ERR with respect to the crack size for linear-elastic structures (Keum and Kwak, 1992; Feijóo et al., 2000; Chen et al., 2001a, b; 2002).[2] For example, Keum and Kwak (1992), and Feijóo et al. (2000) applied the theory of shape sensitivity analysis to calculate the first-order derivative of the potential energy with respect to the crack size. Since ERR is the first-order derivative of the potential energy, the ERR can be calculated by this second approach. Later on, Taroco (2000) extended this approach to formulate the second-order sensitivity of potential energy to predict the first-order derivative of ERR. This is, however, a formidable task since it involves calculation of second-order sensitivities of displacement field. No numerical results were presented (Taroco, 2000). To overcome this problem, Chen et al. (2001a, b; 2002) invoked the domain integral representation of the *J*-integral and an interaction integral and used the material derivative concept of continuum mechanics to obtain the first-order sensitivity of the *J*-integral and mixed-mode SIFs for linear-elastic cracked structures. No mesh perturbation is necessary in the latter approach involving continuum shape sensitivity analysis. However, shape sensitivity methods available today (e.g., de Lorenzi, 1982, 1985; Haber and Koh, 1985; Barbero and Reddy, 1990; Keum and Kwak, 1992; Suo and Combescure, 1992; Hwang et al., 1998; Feijóo et al., 2000; Taroco, 2000; Chen et al., 2001a, b; 2002) are valid only for linear-elastic cracked structures. Since for some materials the nonlinear

[2]The nouns 'derivative' and 'sensitivity' are used synonymously in this paper.

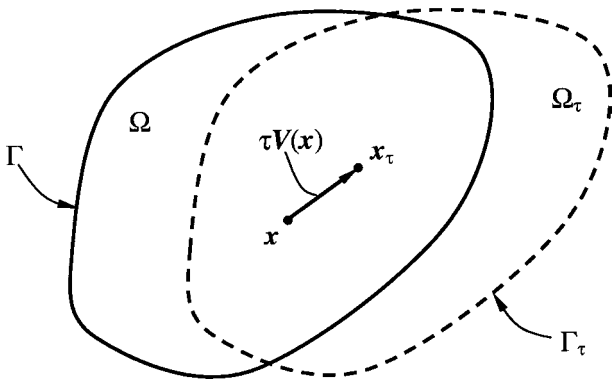

Figure 1. Variation of domain.

fracture-mechanics theory predicts more realistic fracture behavior than the linear-elastic theory, there is a dire need to develop sensitivity equations for nonlinear-elastic cracked structures. To the best knowledge of the authors, no sensitivity methods for nonlinear fracture analysis of cracks are known to have been developed.

This paper presents a new method for predicting the first-order sensitivity of the *J*-integral with respect to crack size in a nonlinearly elastic structure under mode I loading conditions. The method involves the material derivative concept of continuum mechanics, domain integral representation of the *J*-integral, and direct differentiation. Numerical examples are presented to calculate the first-order derivative of the *J*-integral using the proposed method. The results from this method are compared with the finite-difference methods. Based on continuum sensitivities, the first-order reliability method is formulated for predicting the stochastic response and reliability of cracked structures. A fracture reliability problem is presented to illustrate the usefulness of the proposed sensitivity equations.

2. Shape sensitivity analysis

2.1. Velocity Field

Consider a three-dimensional body in its reference or initial configuration. Let $\boldsymbol{\Omega}$ and Γ denote the interior (domain) and the boundary in the initial configuration, respectively. A material point is identified by its position vector $\boldsymbol{x} \in \boldsymbol{\Omega}$. Consider the motion of the body from its initial configuration into a perturbed configuration with domain $\boldsymbol{\Omega}_\tau$ and boundary Γ_τ, as shown in Figure 1. This process can be expressed by

$$\boldsymbol{T}: \bar{\boldsymbol{\Omega}} \to \bar{\boldsymbol{\Omega}}_\tau | \boldsymbol{x}_\tau = \boldsymbol{T}(\boldsymbol{x}, \tau), \tag{1}$$

where the overbar denotes set closure, τ is a real-valued, strictly monotonically increasing function of 'time.' In this study, the parameter τ plays the role of shape-change scalar parameter that defines the transformation $\boldsymbol{T}$, and $\boldsymbol{x}_\tau \in \boldsymbol{\Omega}_\tau$ is the map of $\boldsymbol{x} \in \boldsymbol{\Omega}$ under $\boldsymbol{T}$. At the initial time $\tau = 0$, the domain is $\boldsymbol{\Omega}$. The trajectory of a point $\boldsymbol{x} \in \boldsymbol{\Omega}$, beginning at $\tau = 0$, can now be followed, as shown in Figure 1. The initial point moves to $\boldsymbol{x}_\tau = \boldsymbol{T}(\boldsymbol{x}, \tau)$. Hence, a τ-velocity field, henceforth simply referred to

as the velocity field, can be defined as

$$\boldsymbol{V}(\boldsymbol{x}_\tau, \tau) \equiv \frac{\mathrm{d}\boldsymbol{x}_\tau}{\mathrm{d}\tau} = \frac{\partial \boldsymbol{T}(\boldsymbol{x}, \tau)}{\partial \tau} \tag{2}$$

since the initial point $\boldsymbol{x}$ does not depend on τ. Assuming that $\boldsymbol{T}^{-1}$ exists, i.e., $\boldsymbol{x} = \boldsymbol{T}^{-1}(\boldsymbol{x}_\tau, \tau)$, this velocity field can also be expressed in terms of $\boldsymbol{x}_\tau = \boldsymbol{T}(\boldsymbol{x}, \tau)$, which is

$$\boldsymbol{V}(\boldsymbol{x}_\tau, \tau) \equiv \frac{\mathrm{d}\boldsymbol{x}_\tau}{\mathrm{d}\tau} = \frac{\partial \boldsymbol{T}(\boldsymbol{T}^{-1}(\boldsymbol{x}_\tau, \tau), \tau)}{\partial \tau}. \tag{3}$$

Under common regularity hypothesis, $\boldsymbol{T}$ can be approximated by

$$\boldsymbol{T}(\boldsymbol{x}, \tau) = \boldsymbol{T}(\boldsymbol{x}, 0) + \tau \frac{\partial \boldsymbol{T}(\boldsymbol{x}, 0)}{\partial \tau} + O(\tau^2) \cong \boldsymbol{x} + \tau \boldsymbol{V}(\boldsymbol{x}, 0), \tag{4}$$

where $\boldsymbol{x} = \boldsymbol{T}(\boldsymbol{x}, 0)$. Henceforth, the velocity field $\boldsymbol{V}(\boldsymbol{x}, 0)$ will be simply denoted by $\boldsymbol{V}(\boldsymbol{x})$.

2.2. Material derivative

Let $\boldsymbol{\Omega}$ be a C^k-regular open set, i.e., its boundary Γ is a compact manifold of C^k in $\Re^d (d = 2 \text{ or } 3)$, so that the boundary Γ is closed and bounded in $\Re^d$ and can be locally represented by a C^k function (Fleming, 1965). Let $\boldsymbol{V}(\boldsymbol{x}) \in \Re^d$ in Equation (4) be a vector defined on a neighborhood U of the closure $\bar{\boldsymbol{\Omega}}$ of $\boldsymbol{\Omega}$ and let $\boldsymbol{V}(\boldsymbol{x})$ and its derivatives up to order $k \geqslant 1$ be continuous. With these commonly used hypotheses, it can be shown that for small τ, $\boldsymbol{T}(\boldsymbol{x}, \tau)$ is a homeomorphism (i.e., a one-to-one, continuous map with a continuous inverse) from U to $U_\tau \equiv \boldsymbol{T}(U, \tau)$; $\boldsymbol{T}(\boldsymbol{x}, \tau)$, $\boldsymbol{T}^{-1}(\boldsymbol{x}_\tau, \tau)$, and $\boldsymbol{\Omega}_\tau$ are C^k regular (Zolesio, 1979).

Suppose that $z_\tau, (\boldsymbol{x}_\tau)$ is the classical solution (displacement field) of the governing variational equation from nonlinear elasticity on the perturbed domain $\boldsymbol{\Omega}_\tau$ (Haug et al., 1986)

$$a_{\boldsymbol{\Omega}_\tau}(z_\tau, \bar{z}_\tau) = \ell_{\boldsymbol{\Omega}_\tau}(\bar{z}_\tau), \quad \text{for all } \bar{z}_\tau \in \boldsymbol{Z}_\tau, \tag{5}$$

where z_τ, and $\bar{z}_\tau$, are actual and virtual displacement fields of the structure, respectively, $\boldsymbol{Z}_\tau \subset H^m(\boldsymbol{\Omega}_\tau)$ is the space of kinematically admissible displacements with $H^m(\boldsymbol{\Omega}_\tau)$ denoting Sobolev space of order $m, z_\tau \in \boldsymbol{Z}_\tau \subset H^m(\boldsymbol{\Omega}_\tau)$, $a_{\boldsymbol{\Omega}_\tau}(z_\tau, \bar{z}_\tau) \equiv \int_{\boldsymbol{\Omega}_\tau} \sigma_{ij}(z_\tau)\varepsilon_{ij}(\bar{z}_\tau)\mathrm{d}\boldsymbol{\Omega}_\tau$ and $\ell_{\boldsymbol{\Omega}_\tau}(\bar{z}_\tau) \equiv \int_{\Gamma_\tau} T_i \bar{z}_{i\tau}\, \mathrm{d}\Gamma_\tau$ (assuming no body forces) are the energy form and load linear form, respectively, $\sigma_{ij}(z_\tau)$ and $\varepsilon_{ij}(\bar{z}_\tau)$ are the stress and strain components, respectively, T_i is the ith component of the surface traction, and $\bar{z}_{i\tau}$ is the ith component of $\bar{z}_\tau$. The mapping $z_\tau(\boldsymbol{x}_\tau) \equiv z_\tau(\boldsymbol{x} + \tau \boldsymbol{V}(\boldsymbol{x}))$ in $\boldsymbol{\Omega}_\tau$ depends on τ in two ways. First, it is the solution of the boundary-value problem in $\boldsymbol{\Omega}_\tau$. Second, it is evaluated at a point $\boldsymbol{x}_\tau \in \boldsymbol{\Omega}_\tau$ that moves with τ. Hence, the pointwise material derivative at $\boldsymbol{x} \in \boldsymbol{\Omega}$ can be defined as (Haug et al., 1986)

$$\dot{z} = \dot{z}(\boldsymbol{x}; \boldsymbol{\Omega}, \boldsymbol{V}) \equiv \frac{\mathrm{d}}{\mathrm{d}\tau} z_\tau(\boldsymbol{x} + \tau \boldsymbol{V}(\boldsymbol{x}))|_{\tau=0} = \lim_{\tau \to 0} \left[\frac{z_\tau(\boldsymbol{x} + \tau \boldsymbol{V}(\boldsymbol{x})) - z(\boldsymbol{x})}{\tau} \right]. \tag{6}$$

For $z_\tau \in H^m(\mathbf{\Omega}_\tau)$, Adams (1975) has shown that for a C^k-regular open set $\mathbf{\Omega}_\tau$ and for k large enough, there exists an extension of z_τ in a neighborhood U_τ of $\bar{\mathbf{\Omega}}_\tau$ [3], yielding

$$\dot{z}(\boldsymbol{x}; \mathbf{\Omega}, \boldsymbol{V}) = z'(\boldsymbol{x}; \mathbf{\Omega}, \boldsymbol{V}) + \nabla z^{\mathrm{T}} \boldsymbol{V}(\boldsymbol{x}), \tag{7}$$

where

$$z'(\boldsymbol{x}; \mathbf{\Omega}, \boldsymbol{V}) \equiv \lim_{\tau \to 0} \left[\frac{z_\tau(\boldsymbol{x}) - z(\boldsymbol{x})}{\tau} \right] \tag{8}$$

is the partial derivative of z, and $\nabla z^{\mathrm{T}} \boldsymbol{V} = (\partial z_i / \partial x_j) V_j$ is the convective term with $\nabla = \{\partial/\partial x_1, \partial/\partial x_2, \partial/\partial x_3\}^{\mathrm{T}}$ representing a vector of gradient operator. One attractive feature of the partial derivative is that, given the smoothness assumption, it commutes with the derivatives with respect to $x_i, i = 1, 2,$ and 3, since they are derivatives with respect to independent variables, i.e.,

$$\left(\frac{\partial z}{\partial x_i} \right)' = \frac{\partial}{\partial x_i}(z'), \quad i = 1, 2, \text{ and } 3. \tag{9}$$

Let ψ_1 be a domain functional, defined as an integral over $\mathbf{\Omega}_\tau$, i.e.,

$$\psi_1 = \int_{\mathbf{\Omega}_\tau} f_\tau(\boldsymbol{x}_\tau) \mathrm{d}\mathbf{\Omega}_\tau, \tag{10}$$

where $f_\tau(\boldsymbol{x}_\tau)$ is a regular function defined on $\mathbf{\Omega}_\tau$. If $\mathbf{\Omega}$ is C^k regular, then the material derivative of ψ_1 at $\mathbf{\Omega}$ is (Haug et al., 1986)

$$\dot{\psi}_1 = \int_{\mathbf{\Omega}} [f'(\boldsymbol{x}) + \mathrm{div}\ (f(\boldsymbol{x}) \boldsymbol{V}(\boldsymbol{x}))] \mathrm{d}\mathbf{\Omega}, \tag{11}$$

where $f(\boldsymbol{x})$ is the image of $f_\tau(\boldsymbol{x}_\tau)$ and C^k regular.

2.3. Shape Sensitivity of Response

Consider a general performance measure that can be written in the integral form

$$\psi_2 = \int_{\mathbf{\Omega}_\tau} g(z_\tau, \nabla z_\tau) \mathrm{d}\mathbf{\Omega}_\tau. \tag{12}$$

The material derivative of ψ_2 at $\mathbf{\Omega}$ using Equations (9) and (11) is (Haug et al., 1986)

$$\dot{\psi}_2 = \int_{\mathbf{\Omega}} [g_{,z_i} \dot{z}_i - g_{,z_i} (z_{i,j} V_j) + g_{,z_{i,j}} \dot{z}_{i,j} - g_{,z_{i,j}} (z_{i,j} V_j)_{,j} + \mathrm{div}\ (g \boldsymbol{V})] \mathrm{d}\mathbf{\Omega} \tag{13}$$

for which, a comma is used to denote partial differentiation, e.g., $z_{i,j} = \partial z_i / \partial x_j$, $\dot{z}_{i,j} = \partial \dot{z}_i / \partial x_j$, $g_{,z_i} = \partial g / \partial z_i$, $g_{,z_{i,j}} = \partial g / \partial z_{i,j}$ and V_j is the jth component of $\boldsymbol{V}$. In Equation (13), the material derivative $\dot{z}$ is the solution of the sensitivity equation obtained by taking the material derivative of Equation (5). Note that the expression of $\dot{\psi}_2$ involves

[3] The readers are referred to Adams (1975) for the exact condition on k to have an extension of z_τ in a neighborhood U_τ of $\bar{\mathbf{\Omega}}_\tau$.

field variables evaluated in the initial domain, when ψ_2 is defined in the perturbed domain (see Haug et al., 1986 for further details).

If no body force is involved, the governing variational equation in the initial domain is

$$a_{\mathbf{\Omega}}(z,\bar{z}) \equiv \int_{\mathbf{\Omega}} \sigma_{ij}(z)\varepsilon_{ij}(\bar{z})\mathrm{d}\mathbf{\Omega} = \ell_{\mathbf{\Omega}}(\bar{z}) \equiv \int_{\Gamma} T_i \bar{z}_i \mathrm{d}\Gamma, \tag{14}$$

where $\sigma_{ij}(z)$ and $\varepsilon_{ij}(\bar{z})$ are the stress and strain tensors associated with the actual displacement z and virtual displacement $\bar{z}$, respectively, T_i is the ith component of the surface traction, and $\bar{z}_i$ is the ith component of $\bar{z}$. In Equation (14), the energy form $a_{\mathbf{\Omega}}(z,\bar{z})$ is nonlinear with respect to z and must be linearized for iterative solution of z. If $a^*_{\mathbf{\Omega}}(z;\Delta z,\bar{z})$ denotes the linearized energy form with respect to state variable z and its increment Δz, the incremental form of Equation (14) is

$$a^*_{\mathbf{\Omega}}(z_n^k;\Delta z_n^{k+1},\bar{z}) = \ell_{\mathbf{\Omega}}(\bar{z}) - a_{\mathbf{\Omega}}(z_n^k,\bar{z}), \tag{15}$$

where the subscript n indicates the loading step counter and the superscript k indicates the iteration counter within a loading step. Note, Equation (15) is linear with respect to Δz_n^{k+1}, which can be easily solved (e.g., by solving linear FEM matrix equation) to obtain the total displacement as

$$z_n^{k+1} = z_n^k + \Delta z_n^{k+1}. \tag{16}$$

Equation (16) is solved recursively until the original nonlinear equation (Equation (14)) is satisfied at a given loading step.

Taking material derivative on both sides of Equation (5) and using Equation (11) leads to

$$a^*_{\mathbf{\Omega}}(z;\dot{z},\bar{z}) = \ell'_{\mathbf{v}}(\bar{z}) - a'_{\mathbf{v}}(z,\bar{z}), \quad \forall \bar{z} \in \boldsymbol{Z}, \tag{17}$$

where $a^*_{\mathbf{\Omega}}(z;\dot{z},\bar{z})$ is the linearized energy form that is linear with respect to both z and $\dot{z}$, $\ell'_{\mathbf{v}}(\bar{z})$ and $a'_{\mathbf{v}}(z,\bar{z})$ are the structural fictitious load and external fictitious load, respectively, and the subscript $\mathbf{V}$ indicates the dependency of the terms on the velocity field. Assuming that the state variable z is known as the solution to Equations (15) and (16) at the final converged state of a given loading step, Equation (17) is the linear variational equation of the material derivative $\dot{z}$. In Equation (17), the terms $a^*_{\mathbf{\Omega}}(z;\dot{z},\bar{z})$, $\ell'_{\mathbf{v}}(\bar{z})$ and $a'_{\mathbf{v}}(z,\bar{z})$ can be further derived as

$$a^*_{\mathbf{\Omega}}(z;\dot{z},\bar{z}) = \int_{\mathbf{\Omega}} \frac{\partial \sigma_{ij}}{\partial \varepsilon_{kl}} \varepsilon_{kl}(\dot{z})\varepsilon_{ij}(\bar{z})\mathrm{d}\mathbf{\Omega}, \tag{18}$$

$$\ell'_{\mathbf{v}}(\bar{z}) = \int_{\Gamma} \left\{ -T_i \left(z_{i,j} V_j\right) + \left[(T_i \bar{z}_i)_{,j} n_j + \kappa_{\Gamma} (T_i \bar{z}_i) \right] (V_i n_i) \right\} \mathrm{d}\Gamma, \tag{19}$$

$$a'_{\mathbf{v}}(z,\bar{z}) = -\int_{\mathbf{\Omega}} \left[\frac{\partial \sigma_{ij}}{\partial \varepsilon_{kl}} (z_{k,m} V_{m,l}) \varepsilon_{ij}(\bar{z}) + \sigma_{ij}(z)(\bar{z}_{i,m} V_{m,j}) - \sigma_{ij}(z)\varepsilon_{ij}(\bar{z})\mathrm{div}\boldsymbol{V} \right] \mathrm{d}\mathbf{\Omega}, \tag{20}$$

where, n_i is the ith component of unit normal vector $\boldsymbol{n}$, and κ_Γ is the curvature of the boundary, and $z_{i,j} = \partial z_i / \partial x_j$, $\bar{z}_{i,j} = \partial \bar{z}_i / \partial x_j$, and $V_{i,j} = \partial V_i / \partial x_j$. In Equations (18)

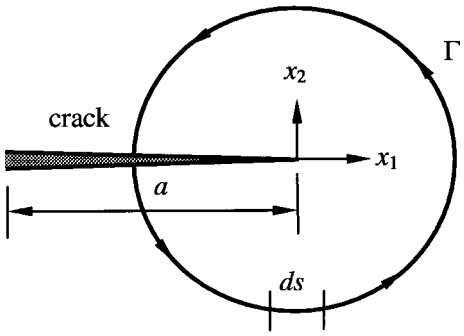

Figure 2. Arbitrary contour around a crack tip.

and (20), $\partial\sigma_{ij}/\partial\varepsilon_{kl}$ can be obtained from the iterative solution at the final converged state of a given loading step.

To perform sensitivity analysis, a numerical method is needed to solve Equation (14) for z. In this study, standard nonlinear FEM was used to solve Equation (14). However, the solution of $\dot{z}$, also required in sensitivity analysis, can be obtained efficiently from Equation (17), since it is actually a linear system. Equation (17) can be solved using the same FEM code or any standard linear equation solver without any iteration. Since the sensitivity equation is always linear even for nonlinear systems, the continuum shape sensitivity method is more efficient than the finite difference method that requires solving at least two nonlinear systems of equations. In this study, the ABAQUS finite element code (ABAQUS, 1999) was employed for all numerical calculations to be presented in Section 5.

3. The *J*-integral and its sensitivity

3.1. The *J*-integral

A widely used constitutive equation for J_2-deformation theory of plasticity (Chen and Han, 1988), usually under small-displacement conditions, is based on the well-known Ramberg-Osgood relation (Anderson, 1995), given by

$$\varepsilon_{ij} = \frac{1+v}{E}s_{ij} + \frac{1-2v}{3E}\sigma_{kk}\delta_{ij} + \frac{3}{2E}\alpha\left(\frac{\sigma_e}{\sigma_0}\right)^{n-1}s_{ij}, \tag{21}$$

where E is Young's modulus, v is Poisson's ratio, σ_0 is a reference stress, α is a dimensionless material constant, n is the strain hardening exponent, δ_{ij} is the Kronecker delta, $s_{ij} = \sigma_{ij} - 1/3\sigma_{kk}\delta_{ij}$ is the deviatoric stress, and $\sigma_e = \sqrt{(3/2)s_{ij}s_{ij}}$ is the von Mises equivalent stress. The deformation theory assumes that the state of stress determines the state of strain uniquely as long as the plastic deformation continues. This is identical to the nonlinearly elastic stress–strain relation as long as unloading does not occur. This paper is concerned with the development of sensitivity equations for the J-integral using only the deformation theory of plasticity (Chen and Han, 1988; Anderson, 1993).

For a cracked body with an arbitrary counter-clockwise path Γ around the crack tip, as shown in Figure 2, a formal definition of the J-integral is (Anderson, 1995)

$$J \equiv \int_{\Gamma} W \mathrm{d}x_2 - T_i \frac{\partial z_i}{\partial x_1} \mathrm{d}s, \tag{22}$$

where $T_i = \sigma_{ij} n_j$ is the ith component of traction vector, n_j is the jth component of unit outward normal to integration path, $\mathrm{d}s$ is the differential length along contour Γ , and $W = \int \sigma_{ij}\, \mathrm{d}\varepsilon_{ij}$ is the strain energy density. For Ramberg–Osgood materials, the strain energy density can be further derived as (Chen, 2001)

$$W = \frac{1+\nu}{3E}\sigma_e^2 + \frac{1-2\nu}{6E}\sigma_e^2 + \frac{n}{n+1}\frac{\alpha}{E\sigma_0^{n-1}}\sigma_e^{n+1}, \tag{23}$$

which provides a useful closed-form expression to be employed in forthcoming equations. For nonlinear-elastic cracked structures, the J-integral uniquely defines the asymptotic crack-tip stress and strain fields, known as the Hutchinson–Rice–Rosengren singularity field (Rice, 1968; Hutchinson, 1983).

3.2. Sensitivity of the J-integral

Under the quasi-static condition, in the absence of body forces, thermal strains, and crack-face traction, the domain form of the J-integral for a two-dimensional crack problem in the perturbed configuration is

$$J = \int_{A_\tau} \left[\left(\sigma_{11}(z_\tau) \frac{\partial z_{1\tau}}{\partial x_1} + \sigma_{12}(z_\tau) \frac{\partial z_{2\tau}}{\partial x_1} \right) \frac{\partial q}{\partial x_1} + \left(\sigma_{21}(z_\tau) \frac{\partial z_{1\tau}}{\partial x_1} + \sigma_{22}(z_\tau) \frac{\partial z_{2\tau}}{\partial x_1} \right) \frac{\partial q}{\partial x_2} - W(z_\tau) \frac{\partial q}{\partial x_1} \right] \mathrm{d}A_\tau, \tag{24}$$

where A_τ is the area inside an arbitrary contour, q is a weight function which is unity at the outer boundary of A_τ and zero at the crack tip. The integrand of the domain integral in Equation (24) can be split as

$$J = \int_{A_\tau} (h_{1\tau} + h_{2\tau} + h_{3\tau} + h_{4\tau} - h_{5\tau}) \mathrm{d}A_\tau, \tag{25}$$

where

$$h_{1\tau} = \sigma_{11}(z_\tau) \frac{\partial z_{1\tau}}{\partial x_1} \frac{\partial q}{\partial x_1}, \tag{26}$$

$$h_{2\tau} = \sigma_{12}(z_\tau) \frac{\partial z_{2\tau}}{\partial x_1} \frac{\partial q}{\partial x_1}, \tag{27}$$

$$h_{3\tau} = \sigma_{21}(z_\tau) \frac{\partial z_{1\tau}}{\partial x_1} \frac{\partial q}{\partial x_2}, \tag{28}$$

$$h_{4\tau} = \sigma_{22}(z_\tau) \frac{\partial z_{2\tau}}{\partial x_1} \frac{\partial q}{\partial x_2} \tag{29}$$

and

$$h_{5\tau} = W(z_\tau) \frac{\partial q}{\partial x_1}. \tag{30}$$

Note, each of the five component integrals in Equation (25) corresponds to the performance measure represented by Equation (12). Assuming the crack length a to be the variable of interest, a change in crack length in the x_1 direction (i.e., mode I loading) only, the velocity field becomes $\boldsymbol{V}(\boldsymbol{x}) = \{V_1(\boldsymbol{x}), 0\}^{\mathrm{T}}$. Hence, using the material derivative formula of Equation (11), the sensitivity of J is given by

$$\dot{J} = \int_A (H_1 + H_2 + H_3 + H_4 - H_5)\mathrm{dA}, \tag{31}$$

where

$$H_i = h_i{}' + \frac{\partial(h_i V_1)}{\partial x_1}, \quad i = 1, \ldots, 5 \tag{32}$$

with h_i representing the image of $h_{i\tau}$. Furthermore, using the general sensitivity formula of Equation (13), the explicit expressions of $H_i, i = 1, \ldots, 5$, can be easily derived and are presented as Equations (A1)–(A5) in Appendix A. The expressions of $H_i, i = 1, \ldots, 5$ in Equations (A1)–(A5), when inserted in Equation (31), yield the first-order sensitivity of J with respect to crack size under mode I loading. All field variables required in calculating the sensitivity of J pertain to the initial configuration. They are valid for both plane stress and plane strain conditions and are applicable to any nonlinearly elastic materials. Further generalization to account for mixed-mode loading and/or to analyze cracks in three-dimensional media is straightforward, as the sensitivity formulation is valid for general three-dimensional structures under arbitrary loads.

The integral in Equation (31) is independent of the domain size and can be calculated numerically using the standard Gaussian quadrature. A 2×2 or higher-order integration rule is recommended for calculating $\dot{J}$. Note that when the velocity field is unity at the crack tip, $\dot{J}$ is identical to a $\partial J/\partial a$. A flow diagram for calculating the sensitivity of J is shown in Figure 3. In Figure 3, $\boldsymbol{K}(\boldsymbol{z}_n{}^k)$ and $\boldsymbol{F}_R(\boldsymbol{z}_n{}^k)$ are the stiffness matrix and load vector, respectively, for displacement $\boldsymbol{z}_n{}^k$ at the kth iteration of the nth loading step, $\boldsymbol{K}(\boldsymbol{z}^*)$ is the stiffness matrix obtained from Equation (18), and the fictitious load $\boldsymbol{F}_{\text{fictitious}}$ $(\boldsymbol{z}^*)$ is the right side of Equation (17), both evaluated at the final converged state $\boldsymbol{z}^*$ of the final loading step.

4. Stochastic fracture mechanics

4.1. Random parameters and fracture response

Consider a mode I loaded nonlinear cracked structure under uncertain mechanical and geometric characteristics subject to random loads. Denote by $\boldsymbol{Y}$ an N-dimensional random vector with components $Y_1, Y_2, \ldots, Y_N$ characterizing uncertainties in the load, crack geometry, and material properties. For example, if the crack size a; far-field applied stress magnitude σ^∞; tensile properties E and α; and mode I fracture toughness at crack initiation J_{Ic}, are modeled as input random variables, then $\boldsymbol{Y} = \{a, E, \alpha, \sigma^\infty, J_{Ic}\}^{\mathrm{T}}$. Let J be a relevant crack-driving force that can be calculated using standard finite element analysis. Suppose that the structure fails when $J > J_{Ic}$. This requirement cannot be satisfied with certainty, since J is dependent on the input

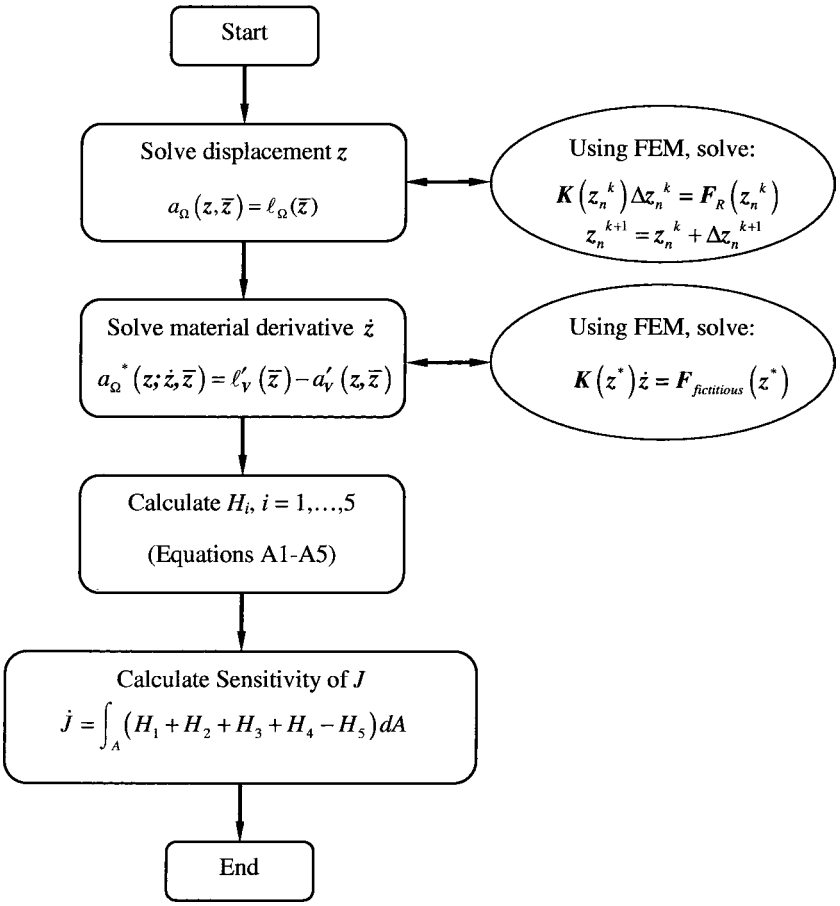

Figure 3. A flowchart for continuum sensitivity analysis of crack size.

vector $\boldsymbol{Y}$ which is stochastic, and J_{Ic} itself is a statistical variable. Hence, the performance of the cracked structure should be evaluated by the probability of failure P_{F}, defined as

$$P_F \equiv \Pr[g(\boldsymbol{Y}) < 0] \equiv \int_{g(\boldsymbol{y})<0} f_{\boldsymbol{Y}}(\boldsymbol{y})\mathrm{d}\boldsymbol{y}, \tag{33}$$

where $f_{\boldsymbol{Y}}(\boldsymbol{y})$ is the joint probability density function of $\boldsymbol{Y}$ and

$$g(\boldsymbol{y}) = J_{Ic}(\boldsymbol{y}) - J(\boldsymbol{y}) \tag{34}$$

is the performance function. Note that P_F in Equation (33) represents the probability of initiation of crack growth, which provides a conservative estimate of structural performance. A less conservative evaluation requires calculation of failure probability based on crack-instability criterion. The latter probability is more difficult to compute, since it must be obtained by incorporating crack-growth simulation in a finite element analysis. However, if suitable approximations of J can be developed analytically, the crack instability-based failure probability can be easily calculated as well (Rahman, 1995). Probabilistic analysis involving crack-instability criterion and shape sensitivity calculations was not considered in this work.

4.2. Reliability analysis by form

The generic expression of the failure probability in Equation (33) involves multi-dimensional probability integration for evaluation. In this study, the first-order reliability method (FORM) (Madsen et al., 1986) was used to compute this probability and is briefly described here to compute the probability of failure P_F in Equation (33) assuming a generic N-dimensional random vector $\boldsymbol{Y}$ and the performance function $g(\boldsymbol{y})$ defined by Equation (34).

The first-order reliability method is based on linear (first-order) approximation of the transformed limit state surface (in the standard Gaussian space), which is tangent to the closest point of the surface to the origin. The determination of this point involves nonlinear constrained optimization and is usually performed in the standard Gaussian image ($\boldsymbol{u}$ space) of the original space ($\boldsymbol{y}$ space). The FORM algorithm involves several steps. First, the space $\boldsymbol{y}$ of uncertain parameters $\boldsymbol{Y}$ is transformed into a new N-dimensional space $\boldsymbol{u}$ consisting of independent standard Gaussian variables $\boldsymbol{U}$. The original limit state $g(\boldsymbol{y})=0$ then becomes mapped into the new limit state $g_U(\boldsymbol{u})=0$ in the $\boldsymbol{u}$ space. Second, a point $\boldsymbol{u}^*$ on the limit state $g_U(\boldsymbol{u}) = 0$ having the shortest distance to the origin of the $\boldsymbol{u}$ space is determined by using an appropriate nonlinear optimization algorithm. This point is referred to as the design point or most probable point, and has a distance

$$\beta = \begin{matrix} \min \\ \boldsymbol{u}\in\Re^N \\ \text{subject to} \end{matrix} \begin{matrix} \|\boldsymbol{u}\| \\ g_U(\boldsymbol{u})=0 \end{matrix} = \|\boldsymbol{u}^*\|, \tag{35}$$

known as the reliability index, to the origin of the $\boldsymbol{u}$ space. Third, the limit state $g_u(\boldsymbol{u})=0$ is approximated by a hyperplane $g_L(\boldsymbol{u})=0$, tangent to it at the design point. Accordingly, the failure probability can be approximated by

$$P_F \cong \Pr[g_L(\boldsymbol{U}) < 0] = \Phi(-\beta), \tag{36}$$

where $\Phi(u)$ is the cumulative probability distribution function of a standard Gaussian random variable. A modified Hasofer–Lind–Rackwitz–Fiessler algorithm (Liu and Kiureghian, 1991) was used to solve the associated optimization problem in this study. The first-order sensitivities were calculated analytically and are described in Section 4.3.

4.3. Analytical gradients

In the $\boldsymbol{u}$ space, the objective function is quadratic; hence, calculation of its first-order derivative with respect to u_k, $k=1,2,\ldots,N$ is trivial. For the constraint function, i.e., the performance function, one must also calculate its derivative with respect to u_k. Assume that a transformation of $\boldsymbol{y}\in\Re^N$ to $\boldsymbol{u}\in\Re^N$, given by

$$\boldsymbol{y} = \boldsymbol{y}(\boldsymbol{u}), \tag{37}$$

exists. The performance function in the $\boldsymbol{u}$ space can then be expressed as

$$g_U(\boldsymbol{u}) = g(\boldsymbol{y}(\boldsymbol{u})) = J_{Ic}(\boldsymbol{y}(\boldsymbol{u})) - J(\boldsymbol{y}(\boldsymbol{u})). \tag{38}$$

Using the chain rule of differentiation, the first-order derivative of $g_U(\boldsymbol{u})$ with respect to u_k is

$$\frac{\partial g_U(\boldsymbol{u})}{\partial u_k} = \sum_{j=1}^{N} \frac{\partial g}{\partial y_j} \frac{\partial y_j}{\partial u_k} = \sum_{j=1}^{N} \frac{\partial g}{\partial y_j} R_{jk}, \tag{39}$$

where $R_{jk} = \partial y_j / \partial u_k$ can be obtained from the explicit form of Equation (37). In nonlinear fracture mechanics with $\boldsymbol{Y} = \{a, E, \alpha, \sigma^{\infty}, J_{Ic}\}^{\mathrm{T}}$ the partial derivatives in the $\boldsymbol{y}$ space are

$$\frac{\partial g}{\partial a} = -\frac{\partial J}{\partial a}, \tag{40}$$

$$\frac{\partial g}{\partial E} = -\frac{\partial J}{\partial E} = \frac{J}{E} (\text{since } J \propto 1/E), \tag{41}$$

$$\frac{\partial g}{\partial J_{Ic}} = 1. \tag{42}$$

For partial derivatives of the J-integral with respect to α and σ^{∞}, it was assumed that the plastic component of J was much larger than the elastic component of J. This assumption is relevant when the elastic strains are much smaller than the plastic strains, which is characteristic of moderate to high loads in a nonlinear-elastic material. Accordingly,

$$\frac{\partial g}{\partial \alpha} = -\frac{\partial J}{\partial \alpha} \approx -\frac{J}{\alpha}, \tag{43}$$

$$\frac{\partial g}{\partial \sigma^{\infty}} = -\frac{\partial J}{\partial \sigma^{\infty}} \approx -\frac{(n+1)J}{\sigma^{\infty}}. \tag{44}$$

When the above assumption is not valid, the partial derivatives of the J-integral with respect to α and σ^{∞} can no longer be approximated using Equations (43) and (44). In the latter case, size sensitivity analysis method must be performed. If required, the derivative of the J-integral with respect to n can also be calculated by the size sensitivity analysis. Size sensitivity analysis, which is simpler than the shape sensitivity analysis developed herein, is not considered in this study.

Using the proposed shape sensitivity method, the partial derivative of J with respect to crack size can be easily calculated. Hence, for a given $\boldsymbol{u}$ or $\boldsymbol{y}$, all gradients of $g_U(\boldsymbol{u})$ can be evaluated analytically, enabling FORM or any other gradient-based reliability analysis to be performed efficiently.

4.4. Interface

Figure 4 illustrates a flowchart of the sensitivity-based FORM for fracture reliability analysis. In solving the optimization problem in FORM, one must be able to calculate $g(\boldsymbol{y})$ for a given $\boldsymbol{y}$. If an external code (e.g., commercial FEM code) is used for finite element analysis, an interface must be developed between the FEM and FORM modules. In addition, if the crack size is random, the crack-tip mesh must be

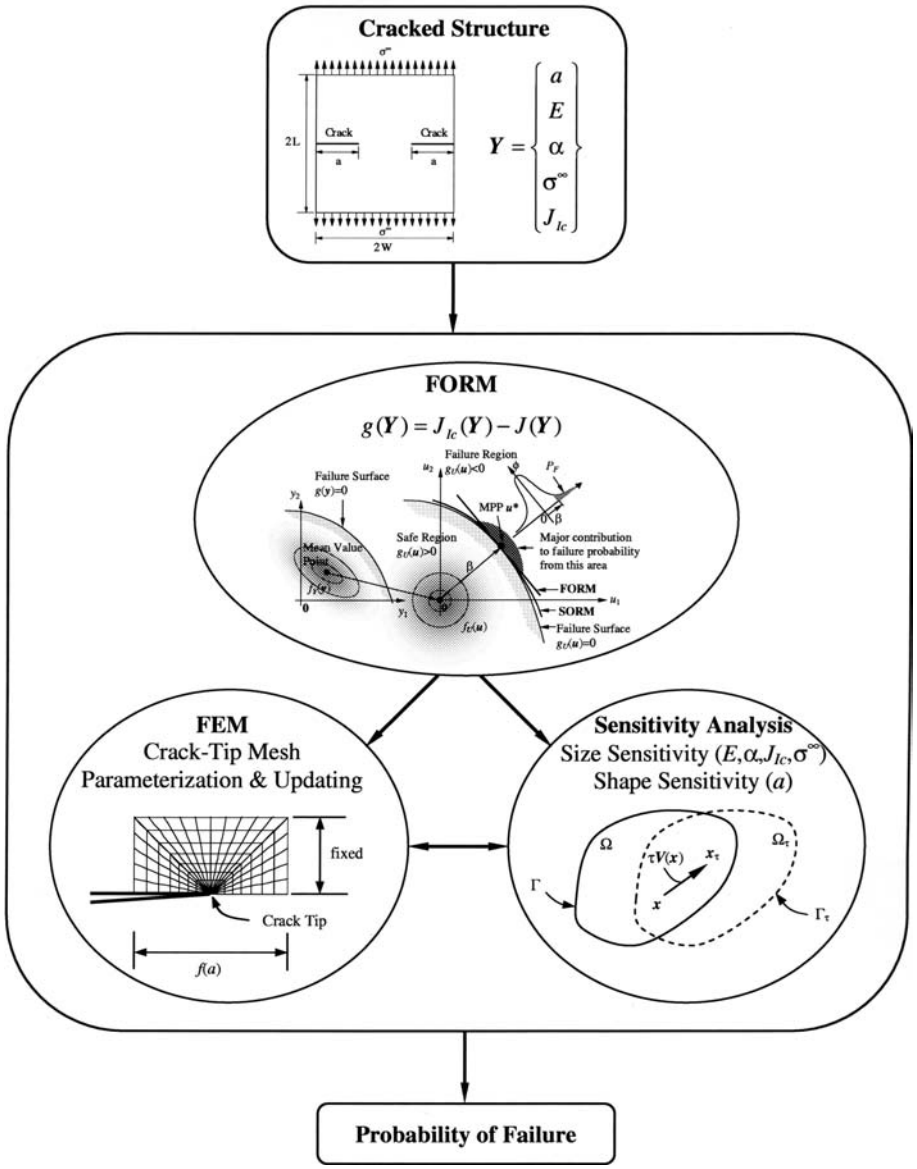

Figure 4. A flowchart for continuum sensitivity-based fracture reliability analysis.

parameterized with respect to crack size parameters, which can be achieved by appropriately modifying the FEM pre-processor module or randomizing the input files of FEM codes. Clearly, there is more than one way to perform such a parameterization. Nevertheless, the crack-tip mesh must be functionally dependent on the crack size such that the mesh quality remains adequate for any realization of crack size and the mapping from crack size to mesh movement is sufficiently smooth so that the performance function is differentiable. The gradients of $g(\boldsymbol{y})$ at any given mesh can be calculated using the sensitivity analysis module, as shown in Figure 4. For such calculations, the sensitivity analysis must also be connected with the external FEM code, as depicted in Figure 4.

4.5. Limitations

The sensitivity and reliability analyses presented in this work are limited to nonlinear-elastic fracture mechanics with small deformation. Under small-scale yielding conditions (small plastic zone), a single fracture parameter, such J-integral, characterizes crack-tip conditions and can be employed as a geometry-independent fracture criterion. However, if there is large-scale plasticity (large plastic zone), single-parameter-based fracture mechanics breaks down. Recall that J characterizes the amplitude of the first and only singular term in a infinite series expansion consisting of several higher-order terms that describe the stress field ahead of the crack tip. The contribution of higher-order terms depends on the distance from the crack tip, the geometry and size of the specimen, and extent of crack-tip plasticity. Elastic–plastic solids with non-proportional loading, unloading, or large-scale plasticity were not considered in this work.

5. Numerical Examples

5.1. Example 1: Sensitivity analysis of M(T) and SE(T) specimens

Consider a middle-tension [M(T)] specimen and a single-edge-tension [SE(T)] specimen with width $2W$ = 1.016 m, length $2L$ = 5.08 m and a crack length $2a$, subject to far-field remote tensile stress σ^{∞} = 172.4 MPa. Two distinct crack sizes with normalized crack lengths, a/W = 0.25 and 0.5 were considered for both M(T) and SE(T) specimens. The material properties of both specimens are: reference stress $\sigma_0 = 154.8$ MPa; elastic modulus E = 207 GPa; Poisson's ratio $v = 0.3$; and Ramberg–Osgood parameters $\alpha = 8.073$ and $n = 3.8$.

Figures 5 and 6 depict the geometry and loads of the M(T) and SE(T) specimens, respectively. A finite element mesh for a half SE(T) specimen model (single-symmetry) and quarter M(T) specimen model (double-symmetry) is shown in Figure 7. A plane stress condition was assumed. Second-order elements from ABAQUS (Version 5.8) (ABAQUS, 1999) element library were used. The element type was CPS8R – the reduced integration, eight-noded quadrilateral element. The number of elements and nodes were 208 and 691, respectively, for the M(T) and SE(T) specimens. Focused elements with collapsed nodes were employed in the vicinity of crack tip. A 2×2 Gaussian integration rule was employed.

Tables 1 and 2 present the numerical results of J and $\partial J/\partial a$ for the M(T) and SE(T) problems, respectively. For each problem, two different crack sizes were analyzed. Two sets of results are shown for $\partial J/\partial a$. The first was computed using the proposed shape sensitivity method; the other employed a finite-difference method. A one-percent perturbation was used in the finite-difference calculations. The results of Tables 1 and 2 show that the continuum sensitivity method provides very accurate results of $\partial J/\partial a$ in comparison with the corresponding results of the finite-difference method. Unlike virtual crack extension techniques, no mesh perturbation is required in the developed method. The difference between the results of the developed method and the finite-difference method is less than four percent.

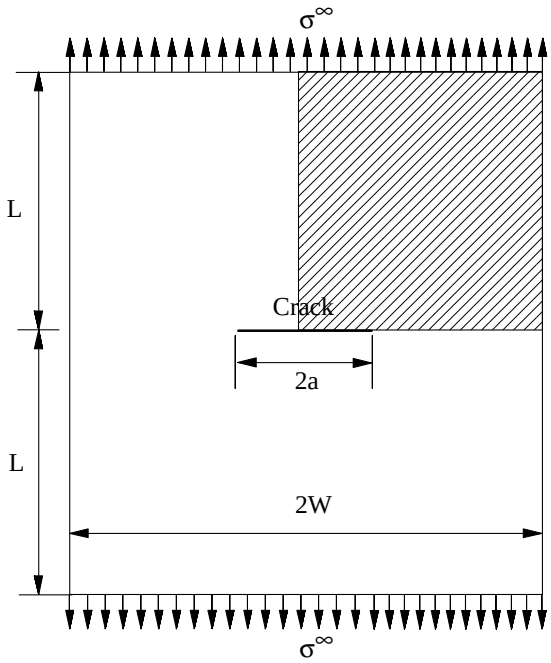

Figure 5. Geometry and loads for M(T) specimen.

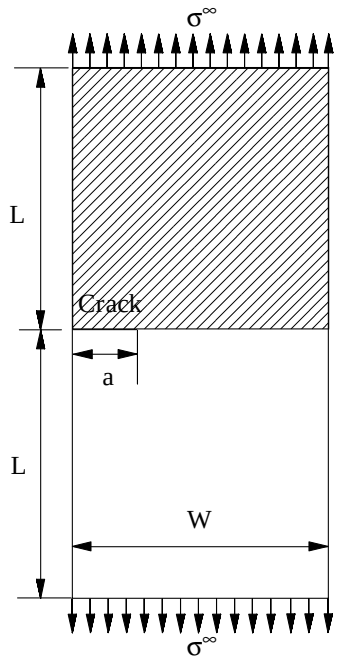

Figure 6. Geometry and loads for SE(T) specimen.

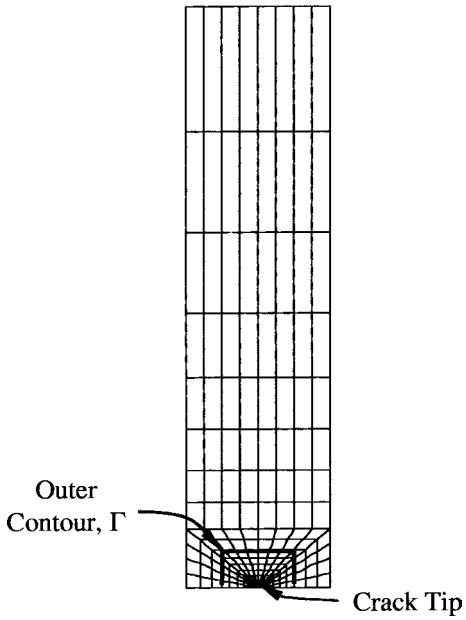

Figure 7. Finite element mesh.

Table 1. Sensitivity of J for M(T) by the proposed and finite-difference methods.

a/W	J(kJ/m^2)	Sensitivity of $J(\mathrm{d}J/\mathrm{d}a)$(kJ/m^3)		Difference (%)
		Proposed method	Finite difference	
0.25	2.0×10^3	27.6×10^3	26.8×10^3	2.87
0.5	11.2×10^3	17.2×10^4	17.6×10^4	−2.73

Table 2. Sensitivity of J for SE(T) by the proposed and finite-difference methods.

a/W	J(kJ/m^2)	Sensitivity of $J(\mathrm{d}J/\mathrm{d}a)$(kJ/m^3)		Difference(%)
		Proposed method	Finite difference	
0.25	6.2×10^3	14.7×10^4	14.4×10^4	1.82
0.5	3.7×10^5	17.1×10^6	16.6×10^6	3.29

5.2. Example 2: Reliability analysis of DE(T) specimen

Consider a double-edge-tension [DE(T)] specimen with width $2W = 1.016\,\mathrm{m}$, length $2L = 5.08\,\mathrm{m}$, and random crack length a, subject to a far-field tensile stress σ^{∞}, as shown in Figure 8. The load σ^{∞}, crack size a/W, and material properties E, α, and J_{Ic} were treated as statistically independent random variables. Table 3 presents the means, coefficients of variation (COV), and probability distributions of these random

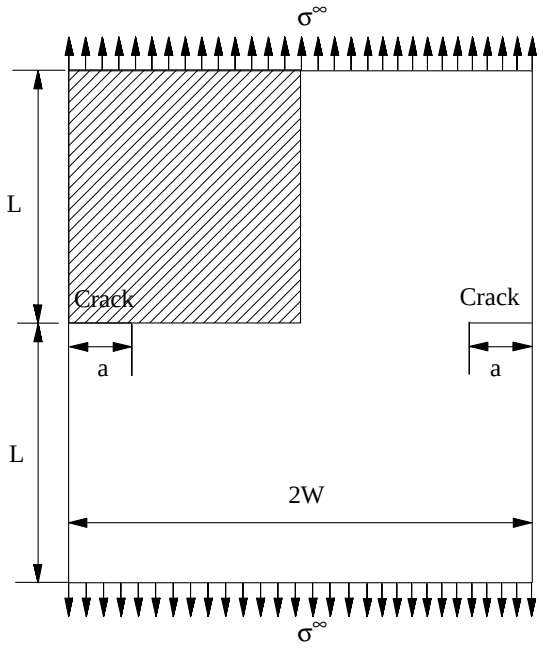

Figure 8. DE(T) specimen under mode I loading.

Table 3. Statistical properties of random input for DE(T) specimen.

Random variable	Mean	COV*	Probability distribution
Normalized crack length (a/W)	0.5	Variable†	Lognormal
Elastic modulus (E)(GPa)	207	0.05	Gaussian
Yield offset (α)	8.073	0.1439	Lognormal
Initiation fracture toughness (J_{Ic})(kJ/m^2)	1243	0.47	Lognormal
Far-field tensile stress (σ^∞)	Variable†	0.1	Gaussian

*Coefficient of variation (COV) = standard deviation/mean.
†Arbitrarily varied.

parameters. The Poisson's ratio $\nu = 0.3$ and the Ramberg–Osgood exponent $n = 3.8$ were assumed to be deterministic.

The finite element mesh illustrated in Figure 7 was also applied for this DE(T) specimen (at mean crack length). Only a quarter of the specimen was modeled due to double-symmetry. A total of 208 elements and 691 nodes were used in the mesh. Second-order elements from the ABAQUS element library were used. The element types are the same as in Example 1. A plane stress condition was assumed. Focused elements were used in the vicinity of crack tip. A 2×2 Gaussian integration rule was used.

Using continuum sensitivity analysis of J, a number of probabilistic analyses were performed to calculate the probability of failure P_F, as a function of mean far-field tensile stress E[σ^∞]. Figure 9 presents the results in the form of P_F vs. E[σ^∞] plots for $v_{a/W}$ = 10 % where $v_{a/W}$ is the COV of the normalized crack length a/W. The probability of failure was calculated using proposed sensitivity-based FORM and

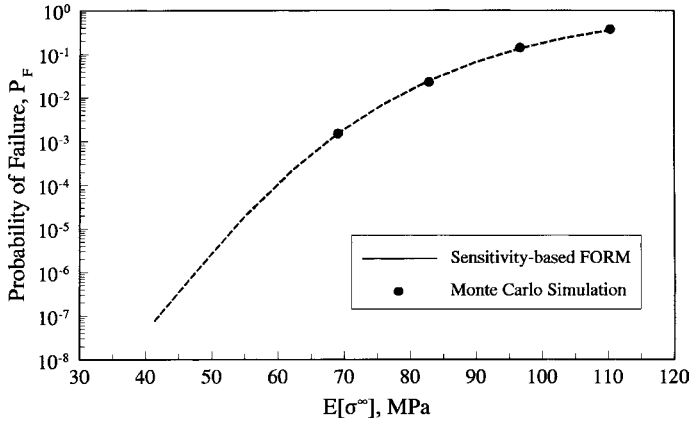

Figure 9. Failure probability of DE(T) specimen by sensitivity-based FORM and simulation.

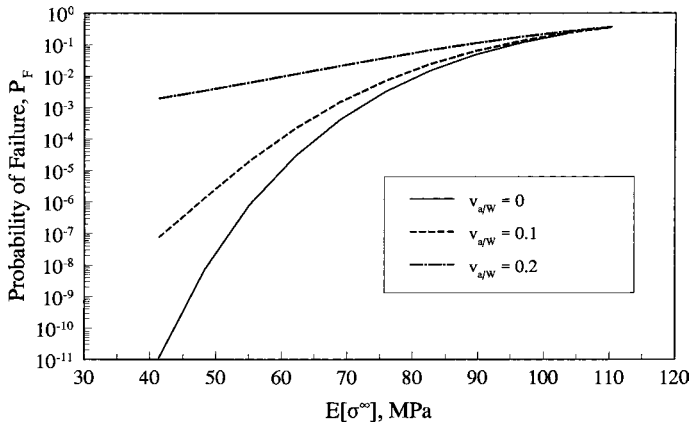

Figure 10. Failure probability of DE(T) specimen for various uncertainties in crack size.

Monte Carlo simulation. For simulation, the sample size varied and was at least 10 times the inverse of the estimated failure probability. As can be seen Figure 9, the probability of failure calculated using sensitivity-based FORM agrees very well with the simulation results.

Figure 10 plots P_F vs. $\mathrm{E}[\sigma^{\infty}]$ for deterministic ($v_{a/W} = 0$) and stochastic ($v_{a/W} =$ 10 and 20%) crack sizes calculated using FORM. The results indicate that the failure probability increases with the COV (uncertainty) of a/W and can be much larger than the probabilities calculated for a deterministic crack size, particularly when the uncertainty of a/W is large. While this trend is expected, the proposed sensitivity formulation allows quantitative evaluation of fracture response and reliability of nonlinear cracked structures. Since all gradients are calculated analytically, the reliability analysis of cracks can be performed accurately and efficiently.

6. Conclusions

A new method was developed for continuum shape sensitivity analysis of a crack in a homogeneous, isotropic, nonlinearly elastic body subject to mode I loading

conditions. The method involves the material derivative concept of continuum mechanics, domain integral representation of the J-integral, and direct differentiation. Unlike virtual crack extension techniques, no mesh perturbation is required in the proposed method. Since the governing variational equation is differentiated before the process of discretization, the resulting sensitivity equations are independent of any approximate numerical techniques. Numerical examples have been presented to illustrate the proposed method. The results show that the maximum difference between the sensitivity of stress-intensity factors calculated using the proposed method and reference solutions obtained by the finite-difference method is less than four percent. Based on the continuum sensitivities, the first-order reliability method was formulated to perform probabilistic fracture-mechanics analysis. A numerical example is presented to illustrate the usefulness of the proposed sensitivity equations for probabilistic analysis. Since all gradients are calculated analytically, the reliability analysis of cracks can be performed accurately and efficiently.

Acknowledgements

This effort was supported by the U.S. National Science Foundation (NSF) Faculty Early Career Development Award (Grant No. CMS-9733058) to S. Rahman.

References

Madsen, H.O., Krenk, S. and Lind, N.C. (1986). *Methods of Structural Safety*. Prentice-Hall Inc., Englewood Cliffs, New Jersey.

Grigoriu, M., Saif, M.T.A., EI-Borgi, S. and Ingraffea, A. (1990). Mixed-mode fracture initiation and trajectory prediction under random stresses. *International Journal of Fracture* **45**, 19–34.

Provan, J.W. (1987). *Probabilistic Fracture Mechanics and Reliability*. Martinus Nijhoff Publishers, Dordrecht, The Netherlands.

Besterfield, G.H., Liu, W.K, Lawrence, M.A. and Belytschko, T. (1991). Fatigue crack growth reliability by probabilistic finite elements. *Computer Methods in Applied Mechanics and Engineering* **86**, 297–320.

Besterfield, G.H., Lawrence, M.A. and Belytschko, T. (1990). Brittle fracture reliability by probabilistic finite elements. *ASCE Journal of Engineering Mechanics* **116**(3), 642–659.

Rahman, S. (1995). A stochastic model for elastic–plastic fracture analysis of circumferential through-wall-cracked pipes subject to bending. *Engineering Fracture Mechanics* **52**(2), 265–288.

Rahman, S. and Kim, J-S. (2000). Probabilistic fracture mechanics for nonlinear structures. *International Journal of Pressure Vessels and Piping* **78**(4), 9–17.

Rahman, S. (2001). Probabilistic fracture mechanics by J-estimation and finite element methods. *Engineering Fracture Mechanics* **68**, 107–125.

Lin, S.C. and Abel, J. (1988). Variational approach for a new direct-integration form of the virtual crack extension method. *International Journal of Fracture* **38**, 217–235.

deLorenzi, H.G. (1982). On the energy release rate and the J-integral for 3-D crack configurations. *International Journal of Fracture* **19**, 183–193.

deLorenzi, H.G. (1985). Energy release rate calculations by the finite element method. *Engineering Fracture Mechanics* **21**, 129–143.

Haber, R.B. and Koh, H.M. (1985). Explicit expressions for energy release rates using virtual crack extensions. *International Journal of Numerical Methods in Engineering* **21**, 301–315.

Barbero, E.J. and Reddy, J.N. (1990). The Jacobian derivative method for three-dimensional fracture mechanics. *Communications in Applied Numerical Methods* **6**, 507–518.

Suo, X.Z. and Combescure, A. (1992). Double virtual crack extension method for crack growth stability assessment. *International Journal of Fracture* **57**, 127–150.

Hwang, C.G., Wawrzynek, P.A., Tayebi, A.K. and Ingraffea, A.R. (1998). On the virtual crack extension method for calculation of the rates of energy release rate. *Engineering Fracture Mechanics* **59**, 521–542.

Keum, D.J. and Kwak, B.M. (1992). Energy release rates of crack kinking by boundary sensitivity analysis. *Engineering Fracture Mechanics* **41**, 833–841.

Feijóo, R.A., Padra, C., Saliba, R., Taroco, E. and Vénere, M.J. (2000). Shape sensitivity analysis for energy release rate evaluations and its application to the study of three-dimensional cracked bodies. *Computational Methods in Applied Mechanics and Engineering* **188**, 649–664.

Chen, G., Rahman, S. and Park, Y.H. (2001b). Shape sensitivity and reliability analyses of linear-elastic cracked structures. *International Journal of Fracture* **112**(3), 223–246.

Chen, G., Rahman, S. and Park, Y.H. (2001a). Shape sensitivity analysis in mixed-mode fracture mechanics. *Computational Mechanics* **27**(4), 282–291.

Chen, G., Rahman, S. and Park, Y.H. (2002). Shape sensitivity analysis of linear-elastic cracked structures under mode-I loading. *ASME Journal of Pressure Vessel Technology* **124**(4), 476–482.

Taroco, E. (2000). Shape sensitivity analysis in linear elastic cracked structures. *Computational Methods in Applied Mechanics and Engineering* **188**, 697–712.

Fleming, W.H. (1965). *Functions of Several Variables*. Addison-Wesley, Reading, Massachusetts.

Zolesio, J.P. (1979). *Identification de Domains par Deformations*. Thèse d Ètat, Université de Nice.

Haug, E.J., Choi, K.K. and Komkov, V. (1986). *Design Sensitivity Analysis of Structural Systems*. Academic Press, New York, NY.

Adams, R.A. (1975). *Sobolev Spaces*. Academic Press, New York, NY.

ABAQUS (1999). User's Guide and Theoretical Manual, Version 5.8, Hibbitt, Karlsson, and Sorenson, Inc., Pawtucket, RI.

Chen, W.F. and Han, D.J. (1988). *Plasticity for Structural Engineers*. Springer-Verlag, New York, NY.

Anderson, T.L. (1995). *Fracture Mechanics: Fundamentals and Applications*. Second Edition, CRC Press Inc., Boca Raton, Florida.

Chen G. (2001). *Shape Sensitivity and Reliability Analysis of Linear and Nonlinear Cracked Structures*. Doctoral dissertation, The University of Iowa, Iowa City, Iowa.

Rice, J.R. (1968). A path independent integral and the approximate analysis of strain concentration by notches and cracks. *Journal of Applied Mechanics* **35**, 379–386.

Hutchinson, J.W. (1983). Fundamentals of the phenomenological theory of nonlinear fracture mechanics. *ASME Journal of Applied Mechanics* **50**, 1042–1051.

Liu, P.L. and Kiureghian, A.D. (1991). Optimization algorithms for structural reliability. *Structural Safety* **9**, 161–177.

Appendix A. The H-functions

The explicit expressions $H_i, i = 1, \ldots, 5$, were derived as follows:

$$H_1 = \frac{\partial z_1}{\partial x_1}\frac{\partial q}{\partial x_1}\left[\frac{\partial \sigma_{11}}{\partial \varepsilon_{11}}\left(\frac{\partial \dot{z}_1}{\partial x_1} - \frac{\partial z_1}{\partial x_1}\frac{\partial V_1}{\partial x_1}\right) + \frac{\partial \sigma_{11}}{\partial \varepsilon_{12}}\left(\frac{\partial \dot{z}_1}{\partial x_2} + \frac{\partial \dot{z}_2}{\partial x_1} - \frac{\partial z_1}{\partial x_1}\frac{\partial V_1}{\partial x_2} - \frac{\partial z_2}{\partial x_1}\frac{\partial V_1}{\partial x_1}\right)\right] + \frac{\partial z_1}{\partial x_1}\frac{\partial q}{\partial x_1}\frac{\partial \sigma_{11}}{\partial \varepsilon_{22}}\left(\frac{\partial \dot{z}_2}{\partial x_2} - \frac{\partial z_2}{\partial x_1}\frac{\partial V_1}{\partial x_2}\right) + \sigma_{11}\frac{\partial q}{\partial x_1}\left(\frac{\partial \dot{z}_1}{\partial x_1} - \frac{\partial z_1}{\partial x_1}\frac{\partial V_1}{\partial x_1}\right), \tag{A1}$$

$$H_2 = \frac{\partial z_2}{\partial x_1}\frac{\partial q}{\partial x_1}\left[\frac{\partial \sigma_{12}}{\partial \varepsilon_{11}}\left(\frac{\partial \dot{z}_1}{\partial x_1} - \frac{\partial z_1}{\partial x_1}\frac{\partial V_1}{\partial x_1}\right) + \frac{\partial \sigma_{12}}{\partial \varepsilon_{12}}\left(\frac{\partial \dot{z}_2}{\partial x_1} + \frac{\partial \dot{z}_1}{\partial x_2} - \frac{\partial z_2}{\partial x_1}\frac{\partial V_1}{\partial x_1} - \frac{\partial z_1}{\partial x_1}\frac{\partial V_1}{\partial x_2}\right)\right] + \frac{\partial z_2}{\partial x_1}\frac{\partial q}{\partial x_1}\frac{\partial \sigma_{12}}{\partial \varepsilon_{22}}\left(\frac{\partial \dot{z}_2}{\partial x_2} - \frac{\partial z_2}{\partial x_1}\frac{\partial V_1}{\partial x_2}\right) + \sigma_{12}\frac{\partial q}{\partial x_1}\left(\frac{\partial \dot{z}_2}{\partial x_1} - \frac{\partial z_2}{\partial x_1}\frac{\partial V_1}{\partial x_1}\right), \tag{A2}$$

$$H_3 = \frac{\partial z_1}{\partial x_1}\frac{\partial q}{\partial x_2}\left[\frac{\partial \sigma_{12}}{\partial \varepsilon_{11}}\left(\frac{\partial \dot{z}_1}{\partial x_1} - \frac{\partial z_1}{\partial x_1}\frac{\partial V_1}{\partial x_1}\right) + \frac{\partial \sigma_{12}}{\partial \varepsilon_{12}}\left(\frac{\partial \dot{z}_2}{\partial x_1} + \frac{\partial \dot{z}_1}{\partial x_2} - \frac{\partial z_2}{\partial x_1}\frac{\partial V_1}{\partial x_1} - \frac{\partial z_1}{\partial x_1}\frac{\partial V_1}{\partial x_2}\right)\right]$$
$$+ \frac{\partial z_1}{\partial x_1}\frac{\partial q}{\partial x_2}\frac{\partial \sigma_{12}}{\partial \varepsilon_{22}}\left(\frac{\partial \dot{z}_2}{\partial x_2} - \frac{\partial z_2}{\partial x_1}\frac{\partial V_1}{\partial x_2}\right) + \sigma_{12}\frac{\partial q}{\partial x_2}\frac{\partial \dot{z}_1}{\partial x_1} - \sigma_{12}\frac{\partial q}{\partial x_1}\frac{\partial z_1}{\partial x_1}\frac{\partial V_1}{\partial x_2}, \tag{A3}$$

and

$$H_4 = \frac{\partial z_2}{\partial x_1}\frac{\partial q}{\partial x_2}\left[\frac{\partial \sigma_{22}}{\partial \varepsilon_{11}}\left(\frac{\partial \dot{z}_1}{\partial x_1} - \frac{\partial z_1}{\partial x_1}\frac{\partial V_1}{\partial x_1}\right) + \frac{\partial \sigma_{22}}{\partial \varepsilon_{12}}\left(\frac{\partial \dot{z}_2}{\partial x_1} + \frac{\partial \dot{z}_1}{\partial x_2} - \frac{\partial z_2}{\partial x_1}\frac{\partial V_1}{\partial x_1} - \frac{\partial z_1}{\partial x_1}\frac{\partial V_1}{\partial x_2}\right)\right]$$
$$+ \frac{\partial z_2}{\partial x_1}\frac{\partial q}{\partial x_2}\frac{\partial \sigma_{22}}{\partial \varepsilon_{22}}\left(\frac{\partial \dot{z}_2}{\partial x_2} - \frac{\partial z_2}{\partial x_1}\frac{\partial V_1}{\partial x_2}\right) + \sigma_{22}\frac{\partial q}{\partial x_2}\frac{\partial \dot{z}_2}{\partial x_1} - \sigma_{22}\frac{\partial q}{\partial x_1}\frac{\partial z_2}{\partial x_1}\frac{\partial V_1}{\partial x_2}, \tag{A4}$$

$$H_5 = \frac{\partial q}{\partial x_1}\frac{\partial W}{\partial \sigma_{ij}}\left[\frac{\partial \sigma_{ij}}{\partial \varepsilon_{11}}\left(\frac{\partial \dot{z}_1}{\partial x_1} - \frac{\partial z_1}{\partial x_1}\frac{\partial V_1}{\partial x_1}\right) + \frac{\partial \sigma_{ij}}{\partial \varepsilon_{22}}\left(\frac{\partial \dot{z}_2}{\partial x_2} - \frac{\partial z_2}{\partial x_1}\frac{\partial V_1}{\partial x_2}\right)\right]$$
$$+ \frac{\partial q}{\partial x_1}\frac{\partial W}{\partial \sigma_{ij}}\frac{\partial \sigma_{ij}}{\partial \varepsilon_{12}}\left(\frac{\partial \dot{z}_2}{\partial x_1} + \frac{\partial \dot{z}_1}{\partial x_2} - \frac{\partial z_1}{\partial x_1}\frac{\partial V_1}{\partial x_2} - \frac{\partial z_2}{\partial x_1}\frac{\partial V_1}{\partial x_1}\right). \tag{A5}$$